A proposal to Jefferson Lab PAC51

A Dark Photon Search with a JLab positron beam

I. EXECUTIVE SUMMARY

A sensitive search for the A′-boson in the mass range from 15 to 90 MeV using the missing mass method.

A. Main physics goals

The goal of the high sensitivity search for the A′-boson [1] is to address the following questions:

- Is the X17 anamoly [2] related to the A′-boson?
- Is there a dark matter boson with a mass in the range of 15-90 MeV?
- Is the A′-boson's effective coupling constant with the electron larger than 10^{-9}?

We propose to search for the A′-boson in the annihilation of a high energy positron with an atomic electron using the missing mass method as discussed for this process in Ref. [3]. Reconstruction of the missing mass from the energy and angle of the detected photon allows us to perform the search **independently of the decay modes** of the A′-boson. The experimental sensitivity does not rely on the coupling of the A′-boson to the quarks or possible semi-visible decay. If the A′-boson signal is observed, the mass will be determined very accurately. A new light gauge boson emerged in supersymmetric extensions of the Standard Model, so a sensitive search proposed here is an important way to find a new fundamental symmetry [1].

B. The proposed measurements/observables

This experiment will detect the photon produced in the reaction. The observed variables are the photon energy and angle relative to the direction of the incident beam. With a total of 60 days of data taking, the projected sensitivity (relative to the QED photon) for the A′-boson for two sigma significance is on the level of 10^{-7} in the mass range of 15 to 90 MeV.

C. Specific requirements on detectors, targets, and beam

The experiment uses a detector package based mainly on the PRad components [4] at a luminosity of 0.7×10^{35} Hz/cm^2. The experiment will use a positron beam with a current of 0.05 μA and energies of 2.2, 4.4 and 11.0 GeV with a 5-cm-long liquid hydrogen target.

D. Resubmissions

The concept of this experiment has been published a few times and reported on at conferences. It is similar to one used in the MMAPS Cornell University proposal to NSF [5] and the VEPP-3 project with an internal target in the storage ring [6]. The LNF PADME experiment [7] is a successful realization of the concept for a 500 MeV beam, but because it is based on a 50 Hz pulsed accelerator, the PADME experiment productivity is limited.

The advantages of the current proposal are due to 100% duty cycle of the beam, high beam energy, very good resolutions of the PbWO-based calorimeter, and the unique rate capability of the FADC250/VXS-based DAQ.

A Dark Photon Search with a JLab positron beam

B. Raydo (co-spokesperson), B. Wojtsekhowski (spokesperson-contact), P. Achenbach, S. Boyarinov, A. Camsonne, P. Degtiarenko, D. Gaskell, J. Grames, W. Henry, D. Higinbotham, I. Jaegle, D. Jones, M. Jones, D. Mack, D. Meekins, R. Michaels, E. Pasyuk, A. Somov, S. Stepanyan, H. Szumila-Vance, S. Taylor, A.S. Tadepalli
Thomas Jefferson National Accelerator Facility, Newport News, VA 23606

A. Gasparian (co-spokesperson), D. Bulumulla
North Carolina A&T State University, NC 27411

N. Liyanage (co-spokeperson), A. Ahmed, X. Bai, G. Cates, H. Nguyen, V. Nelyubin
University of Virginia, Charlottesville, VA 232904

D. Hamilton
SUPA School of Physics and Astronomy, University of Glasgow, Glasgow G12 8QQ, UK

I. Rachek, D. Nikolenko
Budker Institute of Nuclear Physics, 630090 Novosibirsk, Russia

E. King, J. Napolitano
Temple University, Philadelphia, PA 19122

S. Mayilyan, H. Mkrtchyan, A. Shahinyan, V. Tadevosyan
AANL, 2 Alikhanian Brothers Street, 0036, Yerevan, Armenia

D. Dutta
Mississippi State University, Mississippi State, MS 39762

C. Peng
Argonne National Laboratory, Lemont, IL 60439

I. Larin, R. Miskimen
University of Massachusetts, Amherst, MA 01003

T. Averett
College of William and Mary, Williamsburg, VA 23185

L. Gan
University of North Carolina,, Wilmington, NC 28403

M. Khandaker
Sacramento City College, Sacramento, CA 95822

B. Vlahovic
North Carolina Central University, Durham, NC 27707

and the PRad collaboration and the Jefferson Lab Positron Working Group

(Dated: May 17, 2023)

We propose an experiment to search for a new particle, the U/A′-boson, by measurement of the missing mass spectra in the positron annihilation in flight with an atomic electron with one final particle (photon) detected. The missing mass reconstructed from the energy and angle of the detected photon will provide the means for the search for any type of secondary particle produced in the reaction -"production experiment". This experiment has the potential to discover a dark matter particle and has a unique feature: The search sensitivity has no impact from the uncertainty in the boson decay mode and branching value.

The proposed search for a narrow peak in the missing mass spectrum will allow us to find or put an upper limit on the new particle coupling with normal matter (electron/positron). The projected statistical sensitivity for the reduced coupling constant f_e^2/e^2 reaches 5×10^{-8} with 60 days of run at a positron beam current of 50 nA. The result will be very important in dark matter parameter analysis.

CONTENTS

II. INTRODUCTION

The search for an experimental signature of physics beyond the Standard Model is a major effort of modern particle physics, see e.g. [8]. Most of the search activity is focused on possible heavy particles with a mass scale of 1 TeV and above. At the same time, as was suggested by P. Fayet [1, 11], there could be extra U(1) symmetry, which requires a new gauge boson, U, also called the A′-boson. This boson could be light and weakly interacting with known particles through kinetic mixing with the ordinary photon [12]. Strong constraints on the light A′-boson parameters were obtained from electron and muon anomalous magnetic moments $(g-2)$ and particle decay modes [13–17].

Renewed interest in a search for this new gauge boson has been seen recently as such a boson may provide an explanation for various astrophysics phenomena, observed during the last decades, which are related to dark matter [13, 15, 18, 19]. The possible connection between the A′-boson and dark matter in view of the observed slow positron abundance has been investigated for several years and is often referred to as MeV dark matter [20–23].

In the last 15 years, understanding of the particle composition of DM has become a major part of particle physics. The theory of dark matter proposed by N. Arkani-Hamed and collaborators [18], which provided interpretation of a number of key astrophysical observations, has sparked additional interest in an A′-boson search in the mass range below 1 GeV. The latest updates can be found in the recent Snowmass meetings and documents [24–27].

Several methods have been used in the search for the A′-boson signal for the "invisible" decay modes of the A′-boson. The first method uses precise experimental data on exotic decay modes of elementary particles, e.g. $\pi^\circ \to invisible + \gamma$, for the calculation of the upper limit on the A′-boson coupling constant ε to the specific flavor. These upper limits for decay of the J/Ψ and Υ to a photon plus invisible particles were obtained experimentally by means of the "missing particle" approach, where a missing particle in the event type $e^+e^- \to \gamma X$ leads to a yield of events with a large energy photon detected at a large angle with respect to the direction of the positron and electron beams. From the yield of such events the coupling constant could be determined for a wide range of mass of the hypothetical A′-boson. A recent experiment [30] using 53 fb^{-1} of e^+e^- collision data collected with CM energies near the $\Upsilon(2S)$, $\Upsilon(3S)$ and $\Upsilon(4S)$ resonances provided the best data for Υ decay to $\mathrm{A}' + \gamma$ and a limit on the coupling of the A′-boson to the b-quark. In the mass region below 100 MeV the obtained limit for $B(\Upsilon(2S,3S,4S) \to \gamma \mathrm{A}') \times B(\mathrm{A}' \to \text{invisible})$ is $1 \cdot 10^{-6}$; an additional hypothesis of coupling constants' universality is required to get a bound on ε, so direct measurement of the coupling to an electron is of large interest. Currently, the upper limit on the vector coupling obtained from the discrepancy between the calculated electron anomalous magnetic moment and the measured one is $\varepsilon < 1.0 \cdot 10^{-4} \times m_{\mathrm{A}'}[\mathrm{MeV}]$ [15, 16].

A well advanced experimental approach to searching for the A′-boson decaying to invisible states is the missing-energy method, used by the NA64 collaboration at CERN SPS [31]. Such a method provides a very high sensitivity in a wide range of A′-boson mass, but there is a potential problem due to the use of a veto approach, which suppresses observation efficiency in the case of semi-invisible decay. Such decay modes were considered recently [32, 33]. In the missing-energy method the parameters $m_{\mathrm{A}'}$ and ε can not be separately extracted. This limitation is overcome in the LDMX experiment [34], which performs tracking on the recoiling electron. The sensitivity of the LDMX/NA64 method is very high, but specific projections for experimental sensitivity to the A′-boson are include the specific values of the α_D and the ratio $m_{A'}/m_\chi$, which are only theoretical estimates.

For visible decay of the A′-boson, a direct measurement of ε and $m_{\mathrm{A}'}$ could be made by detecting the decay of the A′-boson to an electron-positron pair and reconstructing the e^+e^- invariant mass. This requires a significant branching of A′-boson decay to the e^+e^- pair which is model dependent. A complication of this method is the high level of electromagnetic background in the mass spectrum

of e^+e^-, so such a measurement requires large statistics. Recently, the data sets accumulated in collider experiments have been used for such an analysis [23, 30, 35, 36].

Electron fixed-target experiments, where a new boson decaying to an electron-positron pair can be produced from radiation off an electron beam incident on an external target, are now being widely discussed [17, 37–39, 45].

The significant experimental results on upper limits for a new boson coupling to an electron in the sub-GeV mass range have been reported [40, 41]. A search for the A′-boson in a wide mass range was performed in Ref. [42]. The APEX experiment in JLab Hall A [43] probes couplings $\varepsilon^2 > 10^{-7}$ and masses $m_{A'} \sim 150 - 250$ MeV. The result of the test run, with only 1/100 of the data of the full APEX experiment, has already demonstrated the feasibility of such an approach [41]. Results from the second APEX run are still under analysis. The Heavy Photon Search (HPS) experiment [44] at JLab is in the data taking stage (about halfway finished). Other electron fixed-target experiments are planned: X17 [45] at Jefferson Lab and the MESA facility at Mainz [46].

High energy e^+e^- collider experiments also allow one to do A′-boson searches in the sub-GeV mass range, but with limited sensitivity. At the same time, the mass range below 100 MeV is accessible with a positron beam on a fixed target, see Refs. [3, 6, 7, 9, 10]. In addition, the positron beam with an active thick-target was also proposed for the search for the invisible A′-boson [47, 48].

The positron beam on fixed target experiment PADME, based on the same missing mass method as this proposal, is under way at LNF with a 500 MeV pulse beam from the 50 Hz linear accelerator [7]. PADME is expected to collect statistics which correspond to a sensitivity level of $\varepsilon^2 < 1 \times 10^{-6}$ for the mass range below 20 MeV.

There are several reasons which justify serious present and future experimental efforts to study the dark photon including determination of the mass. In view of the considerations above, it is important to perform all these experiments.

A well tested PRad setup in Hall B [4] will be used in this experiment (with modest changes in the detector and the target) to advance significantly in DM physics.

The text of the proposal is organized as follows: In Section III we describe the physics and in section IV the results of simulation of the missing mass and data analysis. In Section V we describe the experimental approach. In Section VI we describe the data acquisition system. In subsequent sections, we present the proposed measurements (Sec. VII), the expected results and beam time request (Sec. VIII), and the technical considerations related to the equipment (Sec. IX). The proposal concludes with Section X.

III. PHYSICS MOTIVATION

A. Overview

There are several interesting questions that motivate us to explore the process of the positron annihilation in flight:

1. Is the "Atomki" anamoly X17 [2] related to the A′-boson?

2. Is there a dark matter boson with a mass in the range of 15-90 MeV?

3. Is the A′-boson's effective coupling constant with the electron larger than 10^{-9}?

A very significant role in our motivation is due to the universal applicability of the projected results, as it will be sensitive to all types of decay modes of the A′-boson. We will discuss to what level of sensitivity a new boson could be searched for in the proposed measurements. The status of the A′-boson parameter space is shown in Fig. 1 taken from Refs. [27, 28]. Over the seven years since the workshops [28, 29], a number of studies of the visible decay mode have been made. There are also experimental results for the invisible mode from NA64 and a plan has been developed for LDMX. The VEPP-3 and MMAPS projects were canceled. A very large list of DM related studies is available in Ref. [24].

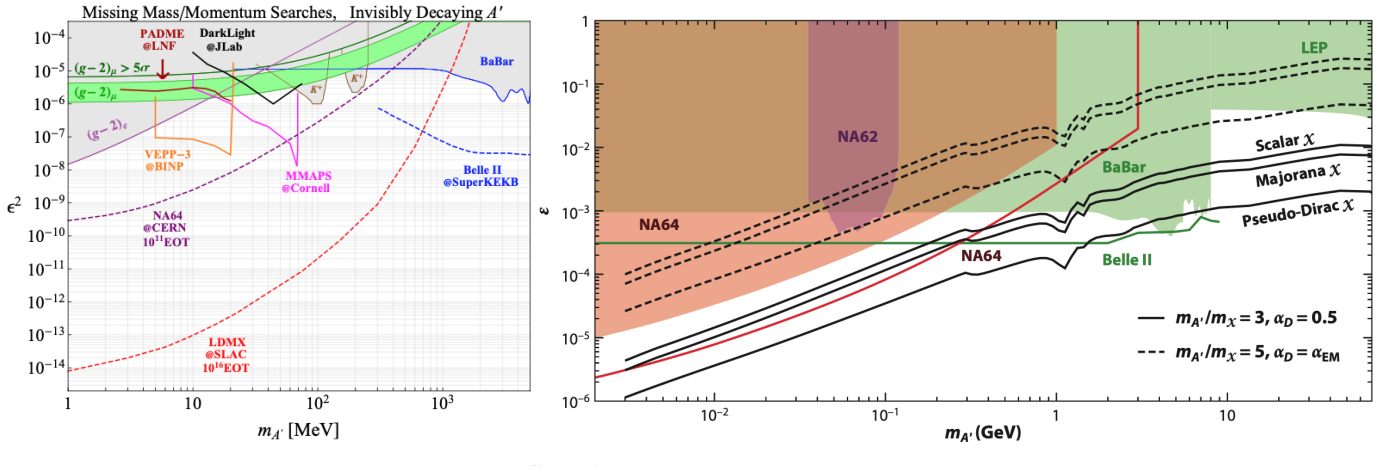

FIG. 1. Parameter space plots for the invisibly decaying A′-boson taken from Refs. [25, 28].

B. A'-boson production

In the proposed experiment we would like to explore the technique of the missing mass with a single-arm photon detector. The concept of this type of experiment is partly described in [3, 6, 10]. A positron beam with an energy E_+ and a liquid hydrogen target make up an "e^+e^- collider". In such a collider it is possible to search for a light A′-boson with a mass of up to $m_{A'}[\mathrm{MeV}] \sim \sqrt{E_+[\mathrm{MeV}]}$. Unlike all other experiments with a fixed target which are based on the detecting of e^-e^+ pairs from A′-boson decay, **in the proposed experiment no special assumptions about decay modes of the A′-boson are required.** In this proposal we consider a medium luminosity ($\sim 0.7\times10^{35}$ cm^{-2}s^{-1}) measurement and a combination of on-line and off-line veto on multi-particle background processes and charged particle hits.

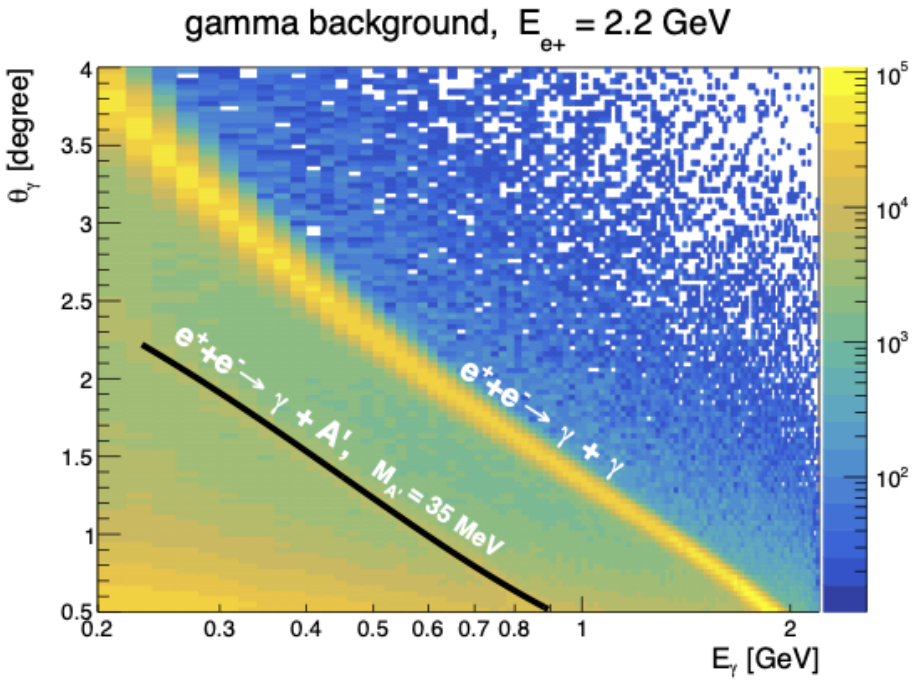

FIG. 2. Two-dimensional distribution of the photon events in the scattering angle and the photon energy for a 2.2 GeV positron beam incident on a hydrogen target. The black band shows the location of A′-boson events of 35 MeV mass.

We are looking for the A′-boson which is the kinetic mixed dark photon. The production of the A′-boson is due to the kinetic mixing operator $\epsilon/2 \cdot F^{Y}_{\mu\nu} F'^{\mu\nu}$, where $F'_{\mu\nu} = \partial_\mu A'_\nu$ and A' is the dark gauge field, see the review in Ref. [25]. A lagrangian of the dark photon $\mathcal{L}_{\mathrm{A}'} = -\frac{1}{4} F'^{\mu\nu} F'_{\mu\nu} + \frac{1}{2}\frac{\epsilon}{\cos\theta_W} B^{\mu\nu} F'_{\mu\nu} - \frac{1}{2} m^2_{A'} A'^{\mu} A'_{\mu}$ allows us to present the production rate of the dark photons (for $m_{A'} \gg m_e$) as:

$$\frac{d\sigma}{d\cos\theta}\,(e^+e^- \to \gamma\, U) \;\simeq\; \frac{\alpha\,\epsilon^2}{s}\left(\frac{1}{\sin^2\theta} - \frac{1}{2}\right)$$

In the process $e^+e^- \to \mathrm{A}'\gamma$ a measurement of the photon energy and its angle allows a reconstruction of the missing mass spectrum and a search for a peak corresponding to the A′-boson. In such a spectrum the dominant rate corresponds to the annihilation reaction $e^+e^- \to \gamma\gamma$ with the reconstructed missing mass peaked at zero. The signal for the A′-boson will be shifted to the area of the continuum (see the illustration in Fig. 2).

The continuum part of the event distribution is dominated by photons emitted in the process of positron scattering from an electron or a proton in the target (bremsstrahlung) and by photons from the three-photon annihilation process. Contributions of other reactions, e.g. $\gamma^\star p \to p\pi^0 \to p\gamma\gamma$, are at least three orders of magnitude smaller than those of the positron bremsstrahlung.

In the proposed experimental setup there is the ability to suppress the QED background significantly, both on-line and off-line, thus improving the sensitivity of the search.

C. The kinematics and cross sections for the signal and background

Two-photon annihilation is the dominant process of high-energy photon production in e^+e^- collisions at a cms energy of a few tens of MeV. The two reactions, depicted in the left panel of Fig. 3, are two-photon annihilation and the production of an exotic A′-boson. The kinematics for the two-

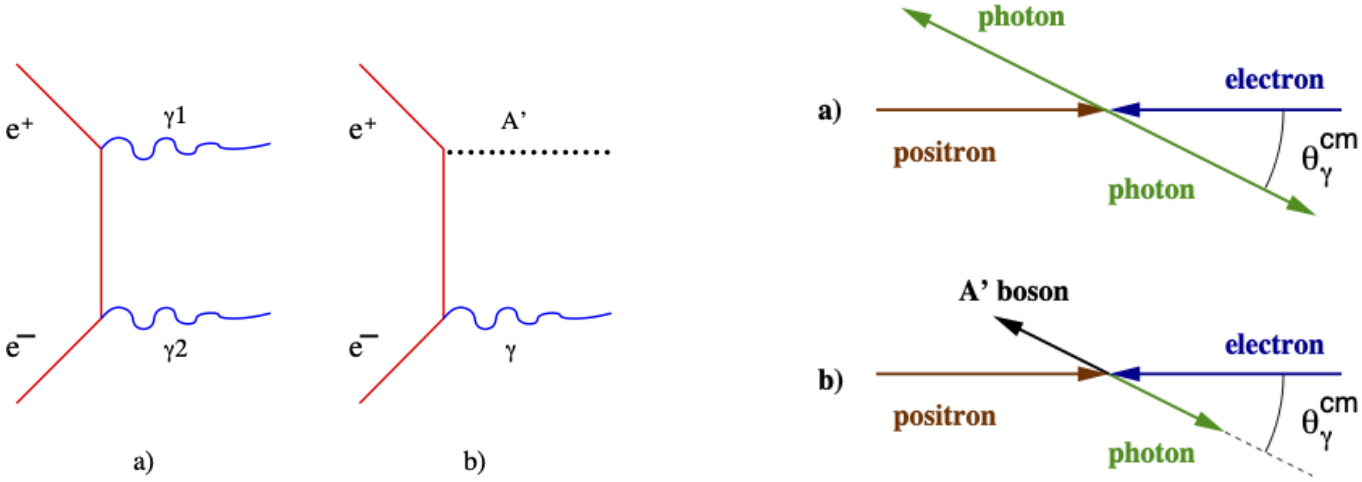

FIG. 3. The diagrams (on the left) and the kinematics (on the right) of a) two-photon annihilation: $e^+e^- \to \gamma + \gamma$, and b) A′-boson production: $e^+e^- \to \mathrm{A}' + \gamma$.

body final state is shown in the right panel of Fig. 3. The energy in the center of mass system $\sqrt{s} = \sqrt{2m^2 + 2E_+m}$, where m is the electron mass and E_+ the positron energy, and the emission angle of the final photon θ_γ with respect to the direction of the positron beam defines the value of the photon energy E_γ. In the case of two-photon production: $E^{lab}_{\gamma(\gamma\gamma)} \approx E_+(1 - \cos\theta^{cm}_\gamma)/2$. In the case of A′-boson production: $E^{lab}_{\gamma(A'\gamma)} = E^{lab}_{\gamma(\gamma\gamma)} \cdot (1 - M^2_{A'}/s)$. The kinematic boost from the center of mass system to the lab leads to a larger photon energy in the forward direction, which helps the measurement of the photon energy. The large variation of the photon energy with the photon angle in the lab system provides an important handle on the systematics.

The energy spectrum of the photons from the two-photon annihilation process in the lab frame is expressed by [50]:

$$\frac{d\sigma}{dy} = \frac{\pi r_e^2}{2\gamma_+ - 2}\left\{\frac{1}{y}\left[1 - y - \frac{2\gamma_+ y - 1}{y(\gamma_+ + 1)^2}\right] + \frac{1}{1-y}\left[y - \frac{2\gamma_+(1-y) - 1}{(1-y)(\gamma_+ + 1)^2}\right]\right\}, \tag{1a}$$

where $y = E^{lab}_\gamma/(E_+ + m)$, with $y_{min} = 1/2\left[1 - \sqrt{(\gamma_+ - 1)/(\gamma_+ + 1)}\right]$ and $y_{max} = 1 - y_{min}$. In the case of high-energy positrons ($\gamma_+ \gg 1$) the expression can be simplified to:

$$\frac{d\sigma}{dy} \approx \frac{\pi r_e^2}{2\gamma_+}\left[\frac{1-y}{y} + \frac{y}{1-y}\right]. \tag{1b}$$

The differential cross section for the process of A′-boson production in the limit of $\gamma_+ \gg 1$ can be derived for the lab frame from [15, Eq.55]:

$$\frac{d\sigma}{dy} \approx \varepsilon^2 \cdot \frac{\pi r_e^2}{y\gamma_+}\left[\frac{(1+\mu)^2}{1-(y+\mu)} - 2y\right], \tag{2}$$

where $\mu = m^2_{\mathrm{A}'}/s$ and here the photon energy is limited by $y < (1 - \mu)$.[62]

The main physical background process producing a single photon, hitting the photon detector, is the positron bremsstrahlung. The differential cross section of this reaction in the case of a thin

hydrogen target can be evaluated using the expression from Ref. [51]:

$$\frac{d\sigma_\gamma}{dyd\Omega_\gamma} = \frac{4\alpha r_e^2}{\pi}\frac{\gamma_+^2}{y}\left\{\frac{2y-2}{(1+l)^2} + \frac{12l(1-y)}{(1+l)^4} + \left[\frac{2-2y+y^2}{(1+l)^2} - \frac{4l(1-y)}{(1+l)^4}\right] \times \left[1 + 2\ln\frac{2\gamma_+(1-y)}{y} - \left(1+\frac{2}{B^2}\right)\ln\left(1+B^2\right)\right]\right\}, \quad (3)$$

where $l = \gamma_+^2\theta_\gamma^2$, $B = 4\alpha\gamma_+(1-y)/y(1+l)$.

However, for the correct reproduction of the γ-quanta angular distribution at $l > 1$, one should consider more accurate formulas for positron-electron elastic (Bhabha) scattering with bremsstrahlung. We employed a simplified version of the approach described in [52].

One more process which produces a non-negligible background rate in the considered search is the three-photon annihilation $e^+e^- \to \gamma\gamma\gamma$. With sufficient accuracy it can be evaluated as a radiative correction to the dominating two-photon annihilation process. We used the prescription from Ref. [53] to account for both $\gamma\gamma$ and $\gamma\gamma\gamma$ annihilation channels in a consistent way.

D. Resolution and rates

The expected mass resolution was directly calculated for the calorimeter parameters shown in Fig. 4. Using these parameters it is easy to estimate that $\delta m/m$ could be as good as 1-2%.

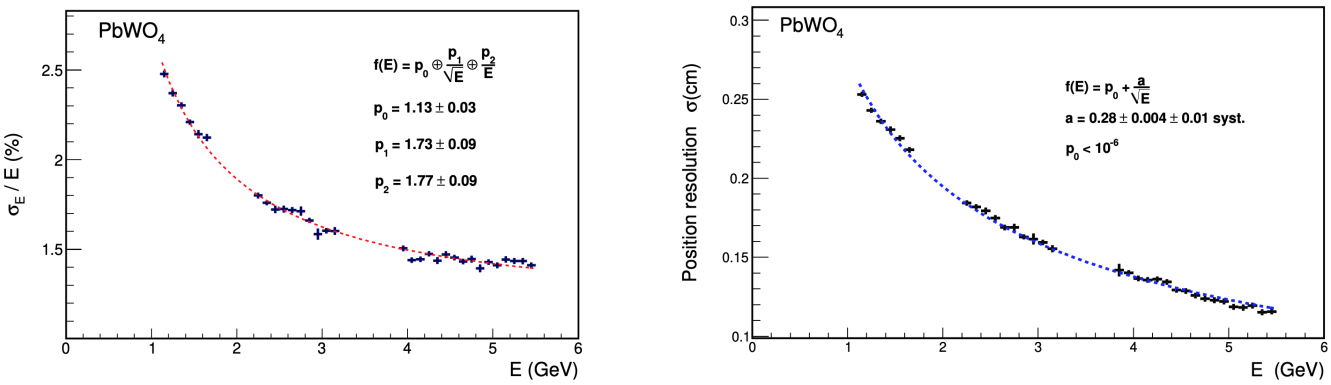

FIG. 4. Observed energy and coordinate resolution of the central section of the HyCal calorimeter.

The rates of beam induced processes such as elastic scattering from a proton and an electron in the target, associated bremsstrahlung, electron-positron pair production by real and quasi-real photons, and positron in-flight annihilation to two and three photons, were calculated using available formulas. The results were compared with MC output with specialized generators as it was done for the VEPP-3 project [6]. Agreement between the two analyses was found to be better than 50%.

Additional validation of the single rates estimate was obtained using the Geant-3-based DINREG simulation of photon and electron yields [54], see Fig. 5. For example, the rate of the MWPC can be estimated from the intensity of electrons for angles above 1° and the solid angle of the relevant area (20 cm^2) $\sim 4 \times 10^{-5}$ sr, which leads to the rate of 0.5 MHz. Considering the MWPC time window of 100 ns, such a counting rate will result in 5% accidentals, so 5% of the neutral particle hits in the calorimeter will be labeled as charged particle hits. For the experiment predictions, we used the results from the full MC program. The rate of the A′-boson is proportional to the two-photon annihilation rate with a coefficient of ϵ^2.

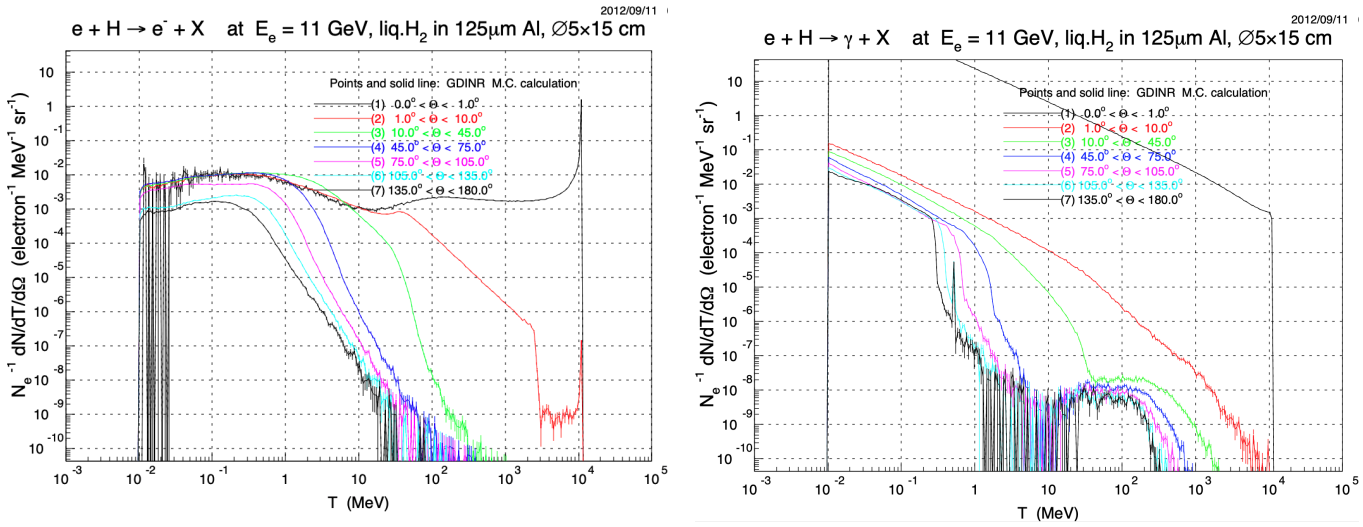

FIG. 5. Electron and Photon rates vs. energy for several angle ranges per DINREG [54].

E. The counting rate of elastic scattering processes

The counting rate from elastic positron scattering from an electron and a proton in the target are about 10 MHz in a small angle area of the calorimeter as illustrated in Fig. 6. These events are very useful for the calorimeter calibration and analysis of the systematics. Using two-cluster events from two charged particles we will be able to test the uniformity of the calorimeter efficiency to the level of a few 10^{-8}. We plan to record a significant part of these elastic events continuously during the data taking run.

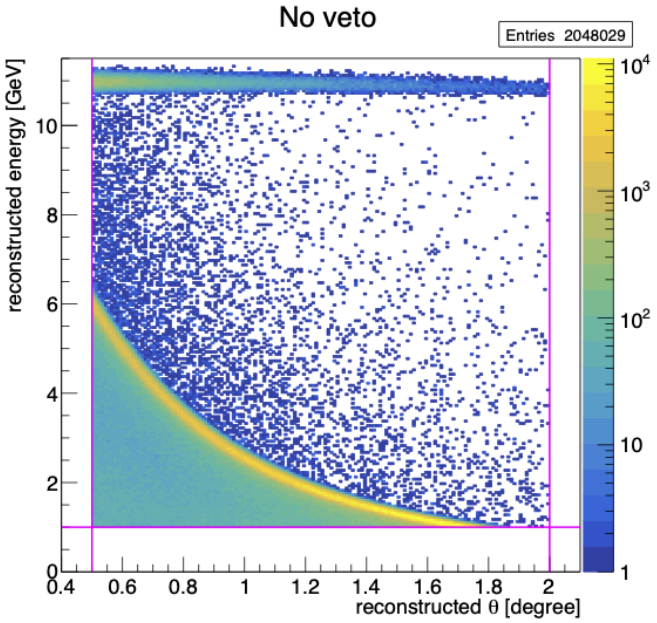

FIG. 6. Energy in the calorimeter vs. scattering angle with the band of the positrons scattered from the proton and the band of positrons(electrons) at lower energy. This plot is for 11 GeV beam energy.

IV. MONTE CARLO SIMULATION

The expected background rates, the strategy of data analysis and the expected search accuracy were analysed using the Monte Carlo simulation of the proposed experimental set up.

The following list of processes was taken into account:

- Single photon bremsstrahlung of positron on proton: The expression 3 is used;
- Single photon bremsstrahlung of positron in elastic (Bhabha) scattering on atomic electrons: A simplified version of the event generator described in [52] is applied;
- Two- and three-photon annihilation: A procedure outlined in Ref. [53] is adopted for the event simulation.
- Elastic electon-proton scattering: The conventional Rosenbluth formula is used for the cross-section.
- The signal process was generated using the cross section formula 2.

No detailed calorimeter response was simulated. The calorimeter is considered as a sensitive area covering the angular range $\theta = 0.5^\circ - 2.5^\circ$ placed at a distance of 700 cm from the target and providing the energy and spatial resolutions taken from the PRad-II paper [4]: $\sigma_{_E}/E = 2.6\%/\sqrt{(E)}$ and $\sigma_x = 0.25$ cm $/\sqrt{E}$.

The task of data analysis is to select events with a single cluster in the calorimeter and no signal in the veto counters and to search for a peak in the missing mass distribution in selected events, so we need to know the experimental resolution for a reconstructed missing mass. Figure 7 shows the results for four values of A′-boson masses when purely A′-boson production events were generated. One can see that the resolution improves rapidly with the increase in the mass of the A′-boson. The dependence can be fitted with an exponential function $\sigma_{Mmiss} = 11\% \cdot e^{-M[\mathrm{MeV}]/35}$ and $\sigma_{Mmiss} = 4.2\% \cdot e^{-M[\mathrm{MeV}]/9.3}$ for the positron beam energy 11 GeV and 2.2 GeV, respectively.

Note that such behavior means that a big tail from two-photon annihilation ($M_{A'} = 0$) is expected in the missing mass spectrum, which indeed is observed. Therefore, for an efficient search at low $M_{A'}$, a strong suppression of two-photon events will be required.

Figure 8 shows the missing mass spectra obtained in the Monte Carlo simulation for $\epsilon^2 = 10^{-2}$. The distribution of missing mass square shown in Fig. 8 also presents decomposition of the background into several categories. The event rates and the contributions of different background processes for the 11 GeV run are accumulated in Table I. The dependence of the event rate on scattering angle θ is demonstrated in Fig. 7.

The simulation data allows direct calculation of the search sensitivity as shown in Fig. 9.

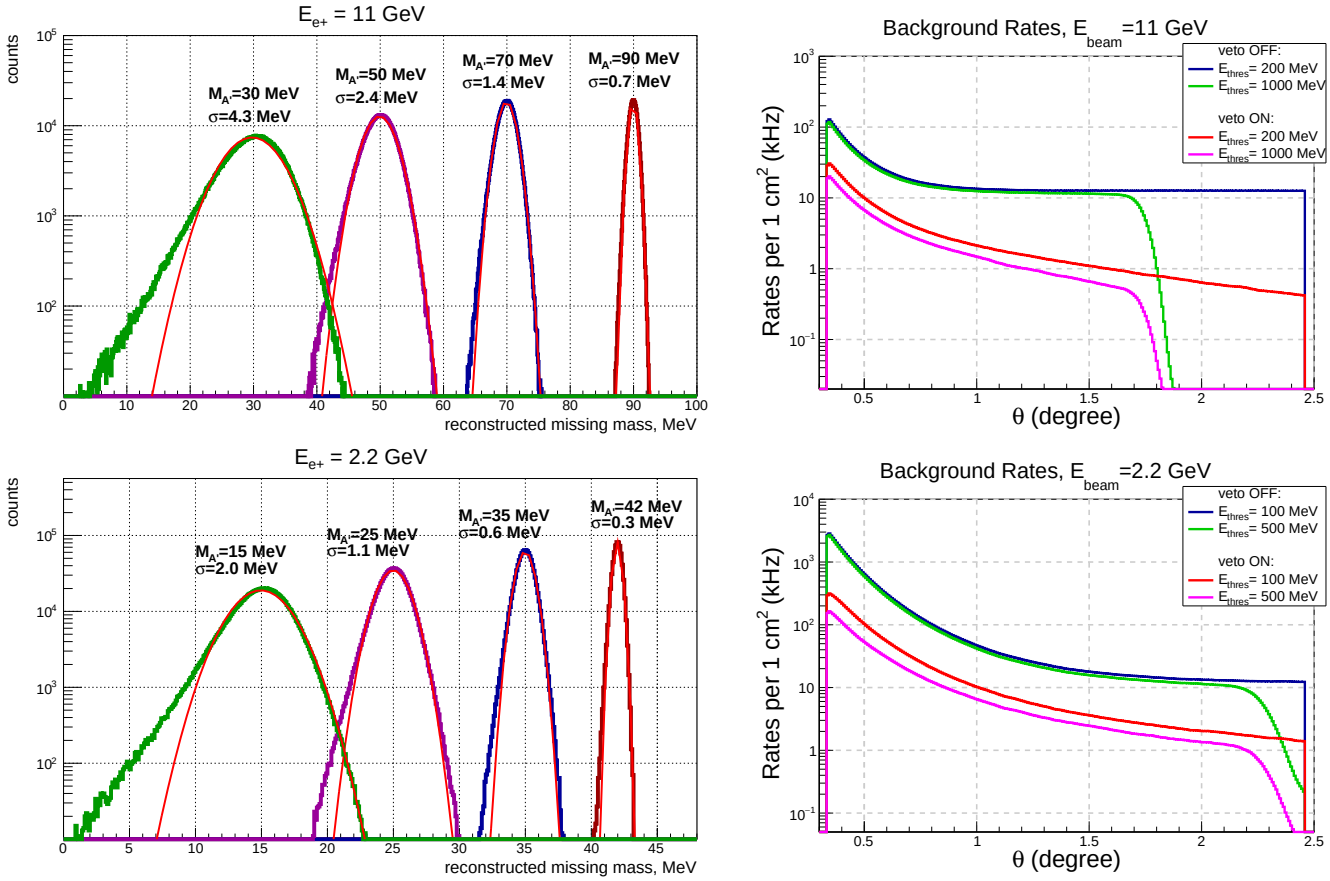

FIG. 7. Left: Monte Carlo simulation of the missing mass resolution for four values of the missing mass. Top plots are for the energy of the positron beam 11 GeV. Right: event rate for two values of the calorimeter energy threshold and with charge veto off/on. Bottom plots are for the energy of the positron beam 2.2 GeV.

TABLE I. Event rates (Hz) for $E_{e+} = 11$ GeV, luminosity $= 7 \times 10^{34} cm^{-2} s^{-1}$, $E_{threshold} = 1$ GeV, $\theta = 0.5^\circ - 2.5^\circ$, $M_{A'} = 80$ MeV, $\epsilon^2 = 1 \times 10^{-7}$.

Whole acceptance

	brems.	$\gamma+\gamma$	$\gamma+\gamma+\gamma$	elastic ep	Bhabha	A'	Total
No cuts	1.57e+05	1.03e+06	3.12e+05	3.85e+05	1.48e+07	3.52e-01	1.67e+07
Charge veto	1.57e+05	1.03e+06	3.12e+05	0.00e+00	2.07e+05	3.52e-01	1.70e+06
Single γ-cluster	1.57e+05	8.87e+05	2.49e+05	0.00e+00	8.73e+04	3.48e-01	1.38e+06

Around $M_{mis} = 80 \pm 1.5$ MeV

	brems.	$\gamma+\gamma$	$\gamma+\gamma+\gamma$	elastic ep	Bhabha	A'	Total
No veto	6.64e+03	0.00e+00	3.94e+03	0.00e+00	6.28e+04	3.04e-01	7.34e+04
Charge veto	6.64e+03	0.00e+00	3.94e+03	0.00e+00	1.38e+04	3.04e-01	2.44e+04
Single γ-cluster	6.64e+03	0.00e+00	3.18e+03	0.00e+00	3.63e+03	3.00e-01	1.34e+04

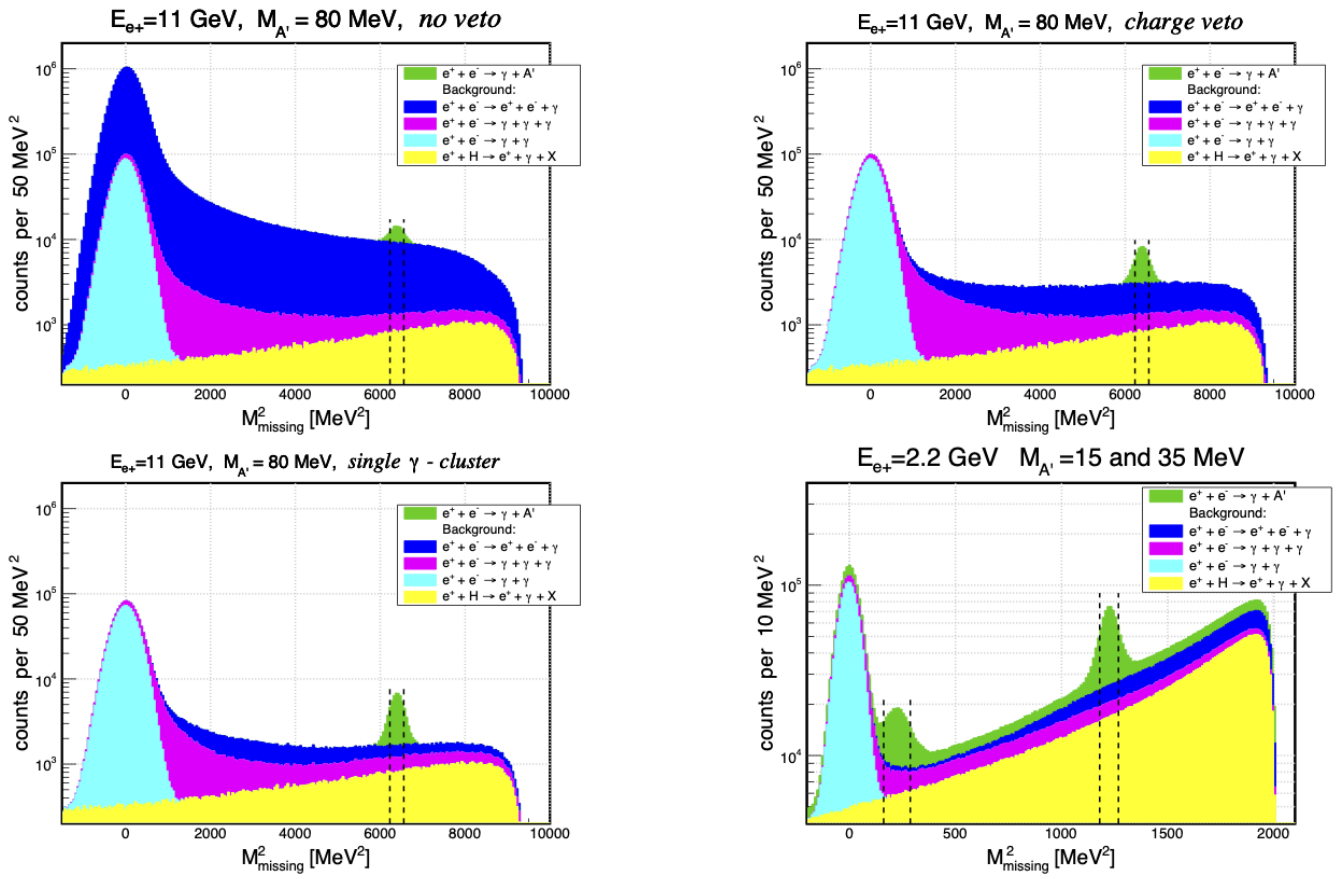

FIG. 8. Results of the Monte Carlo simulation for the missing mass distribution. The mixing constant is taken to be $\epsilon^2 = 10^{-2}$. Top row: $E_{e+} = 11$ GeV, $M_{A'} = 80$ MeV. Left – all events, right – after charge veto turned on. Bottom row: all cuts applied, only single γ-clusters selected. Left – for $E_{e+} = 11$ GeV, $M_{A'} = 80$ MeV, Right – for $E_{e+} = 2.2$ GeV, $M_{A'} = 15$ and $M_{A'} = 35$ MeV. Vertical lines indicate the width of a sliding search window ($\pm 1\sigma_M$). Stacked histograms show contributions of various background processes to the final missing mass spectrum. Each spectrum corresponds to data taking for 1.2 seconds with a luminosity of 0.7×10^{35} cm^{-2}s^{-1}.

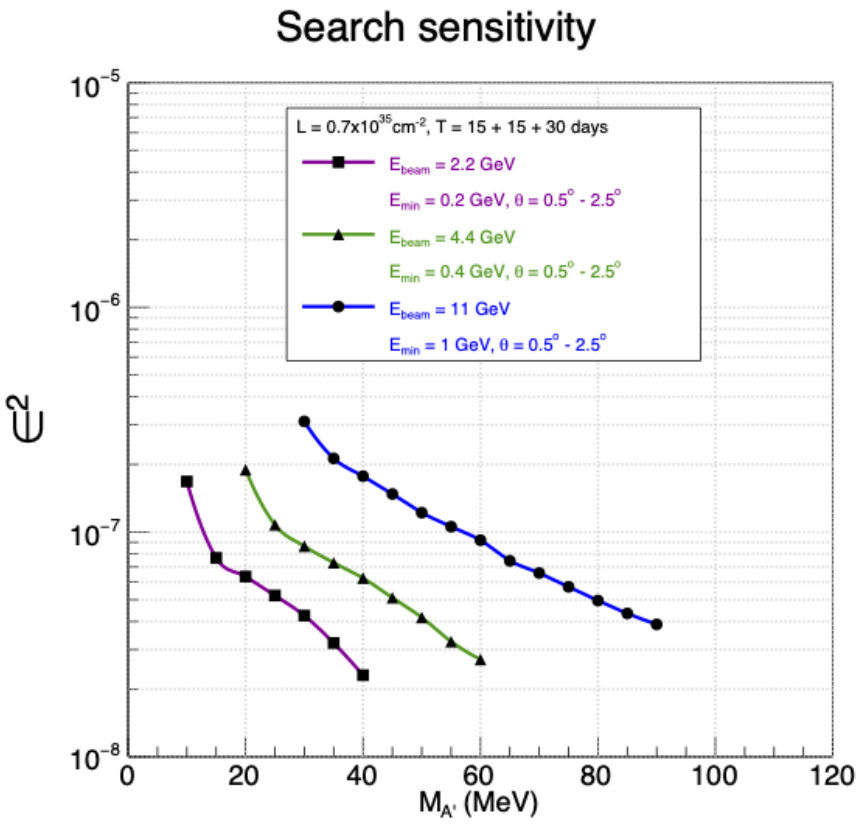

FIG. 9. Monte Carlo simulation of the two-sigma level of sensitivity.

V. EXPERIMENTAL SETUP

The proposed experiment will study photon production by electrons from a liquid hydrogen target, as illustrated in Fig. 10, using the PRad setup and two MWPCs, see also [45]. The setup

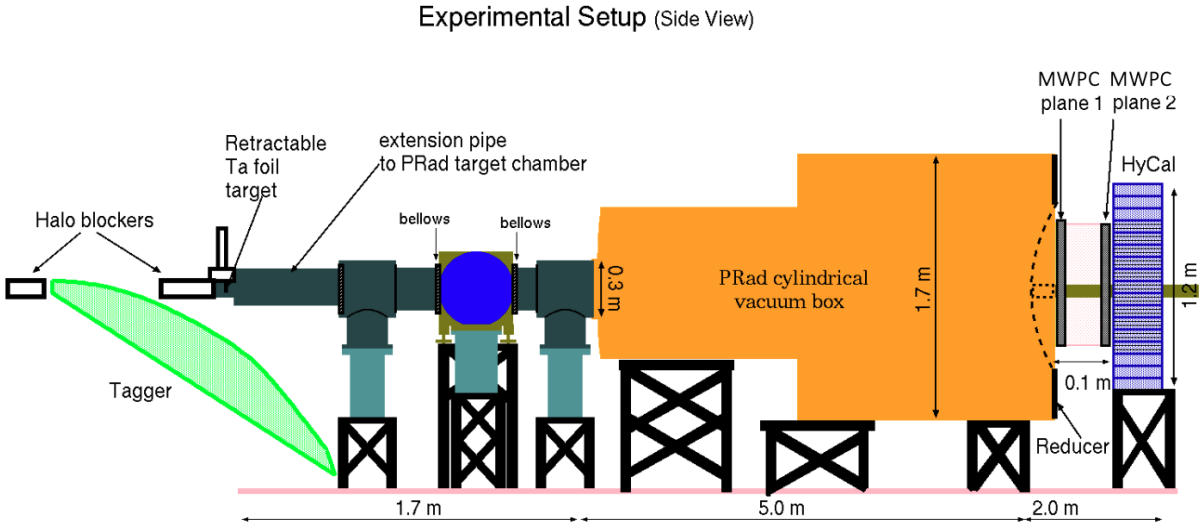

FIG. 10. The layout of the proposed experiment in Hall B. Beam direction is from left to right. The target is located in the blue colored area. Picture is taken from Ref. [45].

includes: the beam halo monitors, the vacuum system, the 5-cm-long liquid hydrogen target, two MWPCs, and the PbWO4-based high resolution calorimeter [56]. The total distance between the LH2 target and the calorimeter face is about 7 m.

Detailed scheme for an A′-boson search experiment have been considered a few times [6, 7] with and without magnetic deflection of the incident beam and a veto of the events which coincide in time with a deflected positron. We found that the use of a veto on a deflected positron is not productive at high luminosity because it puts a strong limitation on the positron beam intensity. Indeed, for a 5-cm-long LH2 target and 50 nA positron beam the low energy tail in the positron spectrum is 5×10^9 Hz for the range $dE/E \sim 1$. In fact, the required range is a bit wider: the $E_{max} = 0.8E_{beam}$ and $Emin \sim 0.1E_{beam}$, see Fig. 2. Thus, the beam bremsstruhlung veto would require reduction of the beam intensity to below 0.5 nA, which leads to a loss in the sensitivity by a factor of 10.

The selected configuration in this proposal does not have magnetic defection but uses a charged veto detector in front of the calorimeter. According to our MC, with the use of such a veto on the charged particle in the useful range of scattered angles (above 0.5 degree), the background rate contribution from the bremsstrahlung events is below 50% of the total background rate and the impact on the signal sensitivity is about $\sqrt{2}$.

A. The PbWO4 calorimeter

The PRad calorimeter, shown in Fig. 11, has been used in several experiments. It has 1152 crystals with dimensions 2x2x18 cm in the central area which we plan to use. The calorimeter has overall size of 119 x 119 cm^2 with the high resolution part of 70x70 cm^2. The DAQ will be upgraded for an already approved set of experiments by using JLab developed FADC250, which allows streaming readout of the data and on-line FPGA-based data analysis.

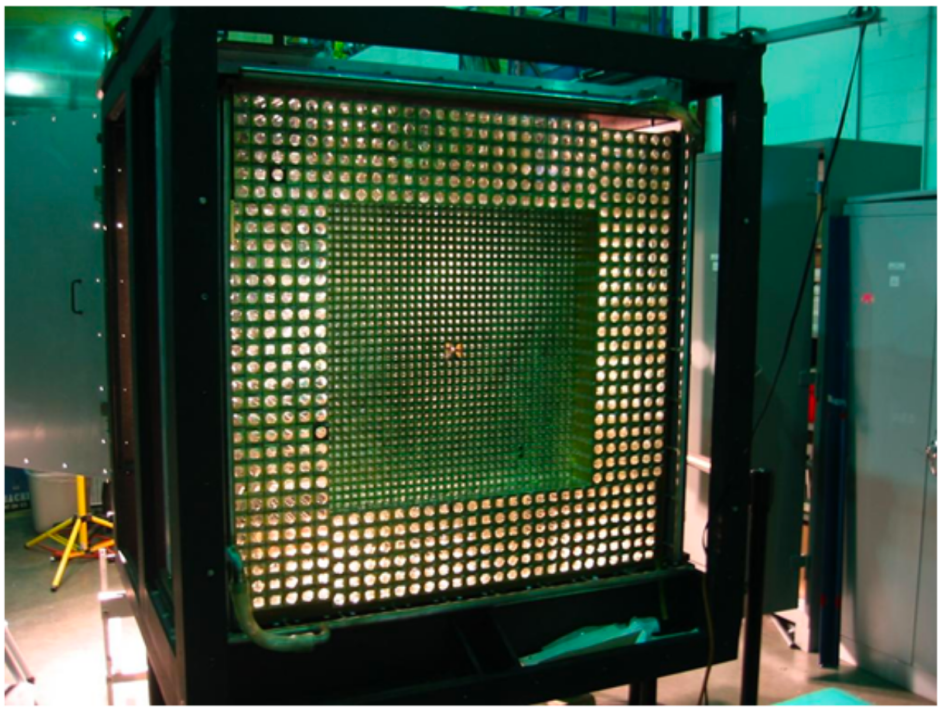

FIG. 11. The front view of the HyCal calorimeter.

The current proposal uses only the existing high resolution section of the calorimeter for calculation of the sensitivity. In the case of a HyCal upgrade and larger size of the high resolution section, a better sensitivity to DM could be achieved.

B. The MWPC

Significant background in this experiment is expected due to electron-positron pair production by the positron beam. We plan to use two MWPCs as a veto detector. The MWPC will be made with 2 mm wire spacing as in Ref. [58]. The 2 mm wire spacing with two-eight adjacent wires interconnected will allow sufficient coordinate resolution and at the same time keep the number of readout channels below 192, which fits in one VETROC VME module. This modest number of channels could be analyzed in the on-line trigger for rejection charged particle hits in the calorimeter. The relatively large time window needed for MWPC (100 ns) is not a problem for the projected counting rate of charged particles.

C. Trigger logic

The signals from the calorimeter will be analyzed in the FADC with time bin 4 ns and a threshold of 100 MeV. The output information for each crystal will have the integral of the signal if that crystal belongs to a cluster with a full cluster energy above the threshold of 300 MeV (for the 2200 MeV beam) and a time stamp for a 100 MeV amplitude crossing. The signals from the MWPCs will be detected in VETROC with a time bin of 20 ns within the time gate of 100 ns relative to the time of the cluster in the calorimeter. The logic of the FPGA analysis is the following: In the first step, we will find a crystal with total energy above 300 MeV (for 2200 MeV beam energy) using FADC signals above the 100 MeV threshold. In the second step, VTP sends back to FADC the IDs for the

crystals which are in the group 3x3 near the crystal with the large amplitude signal and reads from FADC the full integrals for each group of 9 crystals in the cluster. These 3x3 FADC integrals and central crystal timestamp will be packaged in a compact data structure and streamed to the event recorder over Ethernet (further described in the DAQ SYSTEM subsection). All MWPC hits will be streamed to the event recorder over Ethernet.

Each cluster event will contain an integral of the signal, timestamp over threshold, and crystal ID for nine crystals, which amounts in total to less than 100 bytes of data. For a projected rate of less than 20 MHz the data flux is below 2 GB/s, which is already being used in several experiments at JLab.

VI. DAQ SYSTEM

The DAQ system will use standard JLab configured VXS crates, shown in Fig. 12. The HyCal analog signals are digitized with the FADC250 shown in Fig. 13-Left. The MWPC signals from the wires are amplified and discriminated with NINO ASIC cards and digitized with the VETROC shown in Fig. 13-Right. Data from the FADC250 and VETROC modules are streamed to the VTP (Fig. 15) where filtering is done on the HyCal data to reduce the data rate before HyCal and MWPC data are streamed out using up to four 10Gbps Ethernet links, from each readout crate, to the servers for storage. The behavior of these modules and processing procedures are described in the following sections.

A. VXS Crate

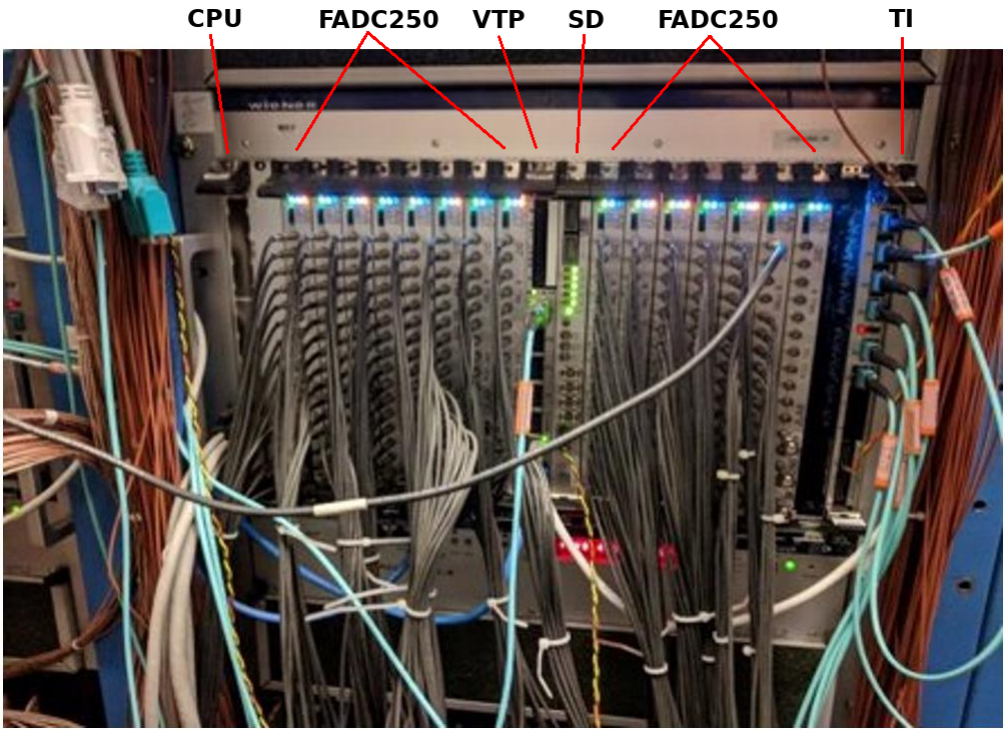

FIG. 12. JLab VXS Crate of FADC250 modules. CPU is used for configuration, VTP for trigger processing and readout, SD to distribute DAQ synchronization signals, TI to receive DAQ synchronization signals from global trigger system.

A 21 slot VXS crate supports up to 16 front-end modules (e.g. 16 FADC250 modules for 256 FADC channels, 16 VETROC modules for 3072 TDC channels, or a mixture of these modules). A CPU is used to configure, monitor, and (optionally) readout front-end modules. The TI and SD modules are responsible for receiving and distributing the global DAQ clock, trigger, and sync signals to all front-end modules so that all front-end modules in the full system (across multiple crates) remain synchronized. The system clock jitter is under 10 ps RMS, contributing negligibly to the timing noise typically achievable by the pulses captured by the FADC250 and TDC modules used at JLab. A VTP communicates with each front-end module with bidirectional high speed serial (10 Gbps to 20 Gbps per module), processes data, and streams data out over up to 4 of its 10 Gbps optical Ethernet ports. The CPU readout speed is limited by VME (200MB/s in total from all

front-ends) and 1Gbps Ethernet ports to roughly 120MB/s. The VTP readout speed is limited by VXS (200MB/s per front-end) and one to four 10 Gbps Ethernet ports which each can transport 1 GB/s.

B. JLab FADC250

The FADC250 is a VME/VXS 16 channel flash analog-to-digital converter module used in many experimental setups at JLab.

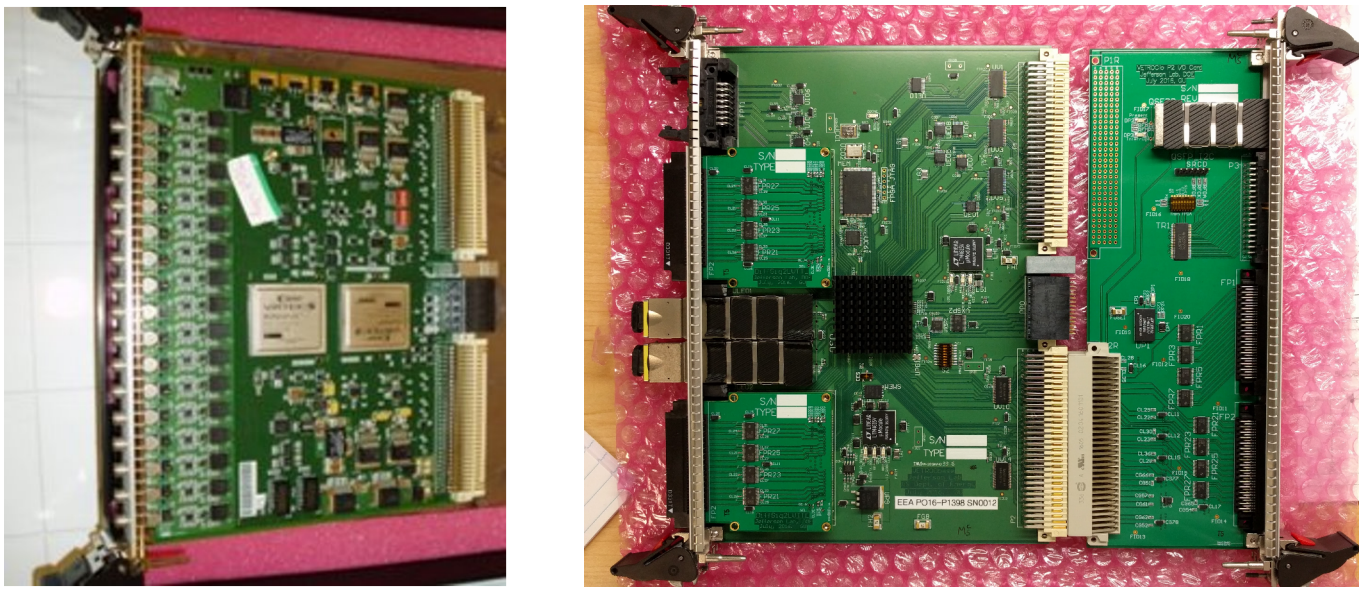

FIG. 13. Left: FADC250 - JLab 16 channel VME/VXS based 250Msps Flash ADC digitizer. Right: VETROC - JLab 128 channel TDC. Expansion/rear transition card that supports an additional 64 TDC channels is shown.

It continuously samples the analog inputs at 250MHz and stores all raw samples in a 8 μs ring buffer, waiting for trigger decisions to choose what to readout. It also detects, integrates, and sends individual pulse charge integrals and timestamps to the VTP over the VXS backplane for readout and/or triggering purposes. This pulse processing on the FADC250 can be seen in Fig. 14.

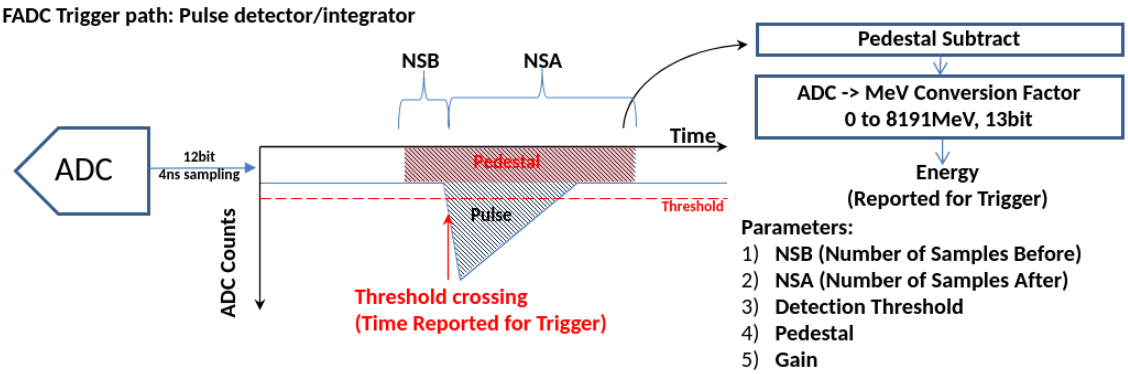

FIG. 14. FADC250 pulse detection, integration, reporting.

C. JLab VETROC

The VETROC (see Fig. 13) is a VME/VXS 128 (up to 192 channels with expansion card) channel TDC (time-to-digital converter). It measures the time of rising and falling edges of digital inputs (ECL, PECL, LVDS) with 1 ns resolution. Hits are stored for up to 16μs in a ring buffer waiting for trigger decisions to choose what to readout (which won't be used in streaming data mode). Hits are also streamed to the VTP using the VXS backplane for readout and/or triggering purposes. Currently the VTP path has a hit timing resolution of 32ns, but this resolution can be improved at the cost of increased dead-time. Additionally, the data to the VTP will be changed to report leading edge time and pulse width together since the NINO provides the measured charge in the form of the pulse width.

D. JLab VTP

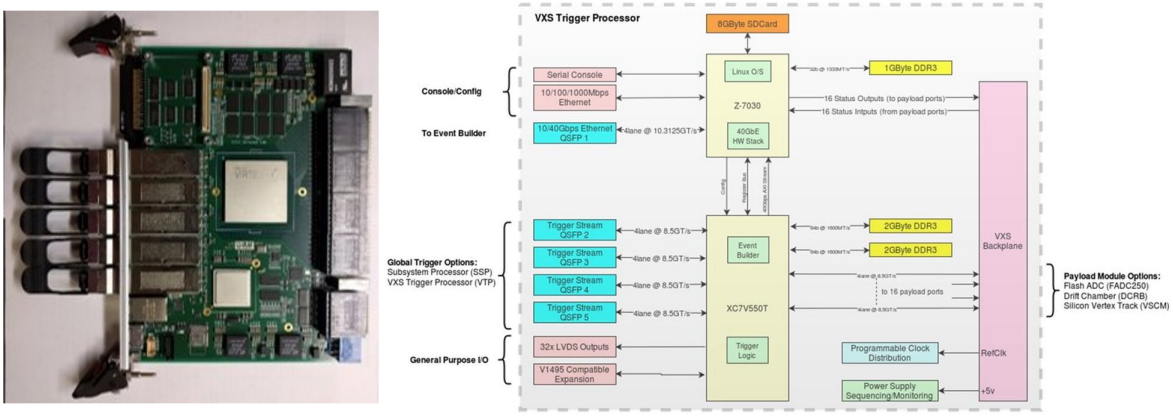

FIG. 15. VTP (VXS Trigger Processor) Module.

The VTP is a switch style VXS board that is connected to all front-end cards over the VXS back using 4 bidirectional serial links that can run up to 8Gbps each. Normally these links run at 3.125 Gbps or 5 Gbps depending on the application, providing from 12.5 Gbps to 20 Gbps bandwidth between each front-end and the VTP. These links are used to stream hits and control information for readout and/or triggering purposes. A XC7V550T FPGA is used to collect the serial streaming, buffer data, and process data. A XC7Z7030T FPGA collects the final readout stream from the XV7V550T and can send it over any of the four 10 Gbps Ethernet optical links using UDP and/or TCP to commericial computers.

E. Streaming and Filtering logic

The VTP receives all FADC250 detected pulses (integrals and 4 ns resolution timestamps) and performs clustering in space and time looking at all 3x3 crystal views in HyCal. The HyCal requires more FADC250 channels than can fit within a single VXS crate - 5 VXS crates and VTPs are needed for HyCal. The VTP shares FADC250 hits along these borders with adjacent crate VTPs so that each VTP can perform 3x3 clustering without missing channels due to the border. This is accomplished using the VTP optical links - there are 4 of them and each can exchange 32 channels over the link.

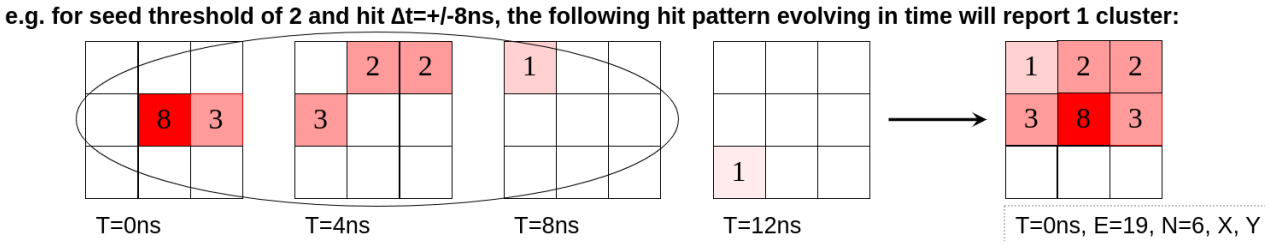

FIG. 16. 3x3 clustering used in filtering.

Hits in the 3x3 cluster view that are within the programmable timing coincidence window are summed and this result is checked against a programmable threshold. The 3x3 clustering is illustrated in the example shown in Fig. 16. When a cluster is found to be over threshold, the VTP sends a fixed latency command back to the FADC250 telling them to report the pulse integrals (without gain or pedestal subtraction applied) for a 5x5 group of channels centered on the initial 3x3 cluster. The VTP collects these 5x5 groups view of pulse integrals and packages this data in a compact form of 25 16-bit values (representing the pulse integrals of all channels in the 5x5 cluster), an 11-bit cluster coordinate, and a 48-bit 4 ns resolution timestamp. This 58-byte packaged cluster data is sent from each VTP with an overall expected cluster rate of 20 MHz resulting in a HyCal cluster data rate of 1.1 GByte/sec, which comfortably fits in the five (up to 20 links available) 10 Gbps Ethernet links used to stream from the VTP (if needed, an additional two 10 Gbps Ethernet links from each VTP are also available). One of the 10 Gbps Ethernet links from each VTP will be used to stream unfiltered VETROC hits from the MWPC.

F. DAQ Crate System Layout

The HyCal crates require special segmentation to allow the system to perform clustering across crate boundaries. The HyCal crate setup is shown in Fig. 17. HyCal is segmented into 5 sections which allow the VTP to be able to exchange FADC hits near the crate boundaries to adjacent VTPs so clustering can be accomplished correctly. Additionally, these optical links will be used to provide the final streamed FADC pulse integrals of clusters to be exchanged so that VTPs can also build a complete cluster event. There are 4 optical links per VTP, which typically run at 20 Gbps, but are scalable to 34 Gbps. The FADC hit shared for clustering requires 34 channels of 16 bits at 31.25 MHz to be exchanged, resulting in 21.25 Gbps utilization (with 8b10b encoding overhead). This requires 2 optical links to be used, which is no problem. The remaining 18.75 Gbps is available for exchanging the final cluster pulse integrals and control information, which is also no problem, for **a total of 20 MHz cluster readout rate**.

The MWPC crate, Fig. 18, will work as a VETROC streaming system with no special filtering. Up to 16 VETROC modules with up to 192 per VETROC supports up to 3k readout channels (far more than needed by MWPC). The VETROC will measure the leading edge hit time from the NINO pulses and also measure the pulse width. Timing resolution is at 1 ns and the information can be stored in a 32-bit word. The resulting hit rate limits are 250 MHz per 10 Gbps Ethernet used by the VTP streaming output (up to 1 GHz hit readout rate using all 4 Ethernet links from the VTP).

The VTP has been used for streaming readout in JLab experiments since 2020, and the DAQ group has implemented support for this system in the CODA framework. Several small scale experiments have used the VTP streaming system, the CLAS12 Forward Tagger Calorimeter and Hodoscope being the first, see Refs. [60, 61].

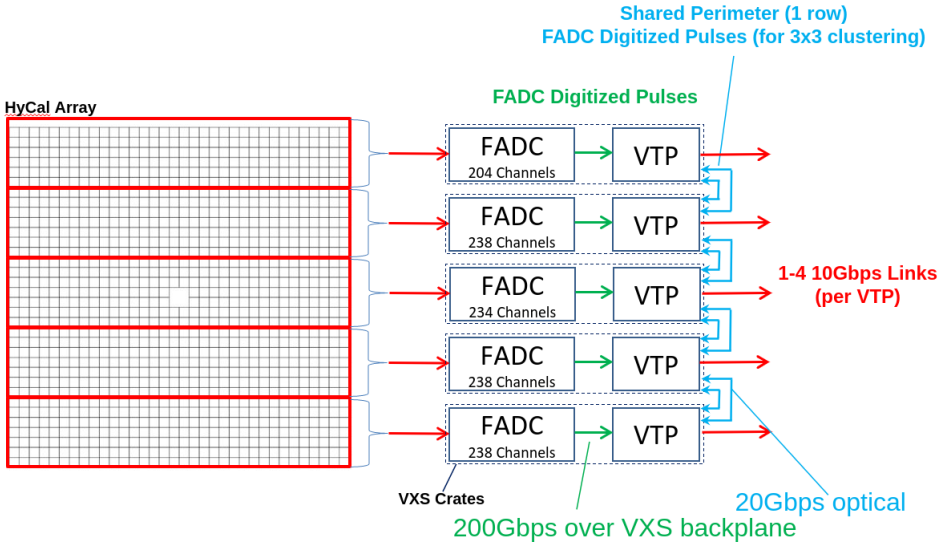

FIG. 17. HyCal DAQ Crate Layout.

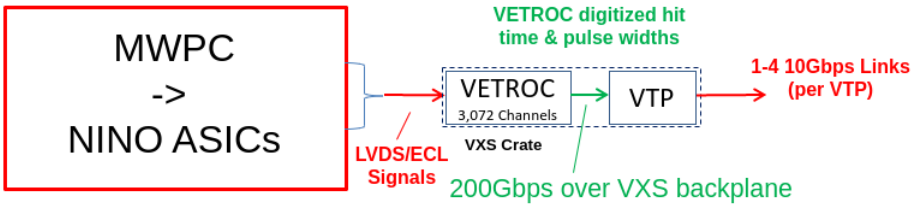

FIG. 18. MWPC DAQ Crate Layout.

G. Conclusion

The dominating data source is the HyCal streaming FADC hits, but with the hit stream filtering we expect no more than 20 MHz of clusters in the energy region of interest. The compact data packing of 58 bytes for the upper limit of 20 MHz of clusters, 1.16 GB/s, is well under the VTP streaming readout bandwidth (5 GB/s planned, with 20 GB/s capacity if ever needed).

VII. PROPOSED MEASUREMENTS

A positron beam with a current of 50 nA at an energy of 2.2, 6.6, and 11 GeV will be used with a 5-cm-long target of liquid hydrogen. The produced particles will be detected in the electromagnetic calorimeter and two MWPCs (for charged particle identification). All features of the experimental technique have been used before at Jefferson Lab or are well developed.

A. The calibration and systematics

The rates of elastic scattering events (from the proton and the electron) are of 5 MHz for e^+-p and 20 MHz for e^+-e^-, mostly in the angular range 0.5-1 degrees. The beam direction and position, the geometry of the calorimeter blocks, and the MWPC will be calibrated by using two-cluster and three-cluster events from elastic scattering and pair production. Calibration of the calorimeter energy response will use both processes, which allows a cross check.

Due to a very high statistics (even after prescaling the charged hits trigger by a factor of three) the accuracy for the geometry parameters will be on the level of 1 nm. Calibration of the efficiency will use two charged particles. The two-cluster events will be used to evaluate the variation of the signal output from the crystals and for preparation of the correction table. The non uniformity of the detector efficiency will be measured to the level of a few 10^{-8}.

The above average rate of a specific crystal will create the bump at one given value of the polar angle and one value of the azimuthal angle (and in both x and y coordinates). By analysis of such distributions we will be able to evaluate and minimize systematics.

An additional direct check will be done by using a locus shown in Fig. 2, which means that a bump at the same mass should appear all along the full range of the locus.

B. Calculation of the experiment sensitivity

Calculation of the signal rate and background rate are presented in Sec. III. The mass resolution was obtained from MC, see Sec. IV. We used the width of the mass range equal to $\pm$ one sigma for determination of $N_{A'}$ - the number of the dark photon events. After the rates and the number of events are found for a given value of ϵ_{MC} the sensitivity limit on the two-sigma level was calculated as: $\epsilon^2 = \epsilon^2_{MC} \times 2 \times \sqrt{N_{background}}/N_{A'}$.

The non uniformity of the detector/DAQ will be on the level of 10^{-8}, so its contribution to the error budget is small.

C. Three production kinematics

The mass resolution has strong variation with value of mass and becomes poor in the lower mass side. Therefore, for the study of the smaller mass region, reduced beam energy leads to higher productivity. We decided to split the run into three beam energy settings which will allow the best overall result for the full mass range.

VIII. EXPECTED RESULTS AND BEAM TIME REQUEST

A. Expected Results

As a result of the production run, the sensitivity to the A′-boson coupling constant $\alpha\,\epsilon^2 \sim 1\times10^{-9}$ will be obtained as shown in Fig. 19.

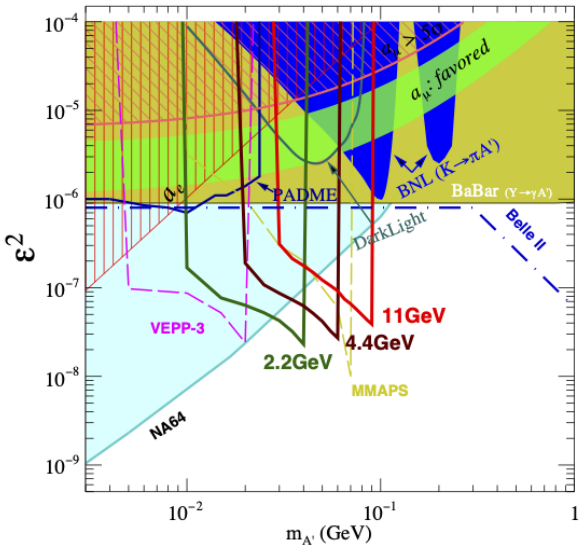

FIG. 19. The parameter space with projected results of this experiment for two sigma exclusion level. The NA64 is shown here; however, its A′-boson detection efficiency may be lower due to the possible semi-invisible decay, e.g. $A' \to \chi + \gamma$, which leads to a loss of A′-boson events.

B. Beam Time Request

The proposed experiment will be done using three different beam energies 2.2, 4.4, and 11 GeV with a positron current of 50 nA. A summary of the requested time is shown in Table II. For the production run we also have the following periods: four shifts for the commissioning of the beam parameters and instrumentation during C1 kinematics, and two shifts per kinematics for the calibration of the calorimeter with e^+-p and e^+-e^- elastic events. The total time requested is a sum of one shift for the DAQ code concept test run (during PRad-II), the required production beam time and the detector/beam calibration time. The total request for this proposal is 60 days.

Kin. #	Beam energy, GeV	Beam, μA	Mass range, MeV	Time, days
C0	2.2	0.04 e^-	DAQ code	1/3
C1	2.2	0.05 e^+	15-40	14 2/3
C2	4.4	0.05 e^+	40-60	15
C3	11	0.05 e^+	60-90	30
	Total requested time			60

TABLE II. The beam time request for the A′-boson experiment.

The lower mass range could be investigated with even higher sensitivity using a 1.1 GeV beam energy. In just 7 days of running, if such a beam becomes available, the sensitivity will be better

than 10^{-7}. It is easy to see that if a beam of 20 GeV becomes a reality at CEBAF, the mass range of the search could be extended to 140 MeV.

IX. TECHNICAL CONSIDERATIONS

A. Time line of development

We expect to run this experiment when the positron beam is available, which is likely to be after the X17 experiment [45] when the calorimeter and its DAQ are fully operational. We will replace the FPGA program in the VXS crates of FADC with a new one needed in this experiment (see sec. VI). The thin foil target of the X17 experiment will be replaced by a cryogenic 5-cm-long cell filled with liquid hydrogen by using cryogenic lines from the PRAD experiment. The GEM-based tracker of the X17 experiment will be replaced by two wire chambers to reduce data volume and allow on-line use of the data to veto clusters in the calorimeter from the charged particles.

B. The technology of the calorimeter, the proportional wire chambers, and DAQ

The technology of the calorimeter and vacuum system were developed for PRad/PimEx, see Ref. [55]. There are plans to increase the size of the high resolution section of HyCal, which will allow us to bump significantly the distance from the target to the detector and improve the missing mass resolution.

The MWPC will be made with 2 mm wire spacing as in Ref. [58]. Each group of five adjacent wires will be interconnected and used for readout. This will allow sufficient coordinate resolution and compact readout with a small number of readout channels. The front-end cards [59] (available from the HRS VDC system) will provide output signals on the LVDS level. Required for MWPC readout, the VETROC modules are available from the GEp CDET DAQ system. The expected cost of the MPWCs construction is $100k.

The composition of the DAQ components is presented in Sec. VI.

C. Installation time

We expect that the installation time for the cryotarget, the MWPCs and the DAQ modification will be two months or less.

D. The CEBAF positron beam

The key for this experiment is a positron beam whose development at JLab has become very active. We plan to use a modest positron beam intensity of 50 nA. Such an intensity is well within the range of the projected parameters [57]. The beam halo is projected to be very small due to the adiabatic damping of the transverse spread in the beam realized at CEBAF. The halo monitors will be used to evaluate the beam quality.

E. Collaboration

The collaboration includes a large group of scientists from all four halls of the JLab physics division, also the positron source group, and the fast electronics group. It includes experts who have succeeded with the PrimEx and PRad experiments. The collaboration also includes a number of colleagues from the international physics community.

X. CONCLUSION

We request 60 days of beam time to do a search for the A′-boson in the missing mass spectrum in the reaction $(e^+ + e^- \rightarrow \gamma)$X.

This experiment will take place in Hall B, utilizing a low intensity positron beam, a PbWO4 calorimeter to detect photons, and two multi-wire proportional chambers for charged particle identification. This will be the first high productivity experiment to measure A′-boson production in positron-electron annihilation in the mass range below 100 MeV which has sensitivity independent of the A′-boson decay physics.

Experiment requirements for positron beam parameters 50 nA (unpolarized) are well within in the scope of the positron beam project [57].

Knowledge of the A′-boson mass and the coupling constant to an electron (or an upper limit of such a coupling) is of large interest to the dark matter research field. The projected statistical uncertainty of the sensitivity is about two standard deviations for the value of coupling 10^7 times smaller than it is for the QED photon. Such sensitivity will also allow us to resolve the question of connection between the X17 particle and A′-boson.

[1] P. Fayet, Phys. Lett. **B 95**, 285 (1980), *Nucl. Phys.* **B 187**184 (1981)
[2] A. Krasznahorkay *et al*, Phys. Rev. Lett. **116**, 042501 (2016)
[3] B. Wojtsekhowski, report at Mini-symposium "Identifying Dark Matter II: Axionic and Sterile Dark Matter" at DNP/APS meeting, Nashville, October 25-28, 2006; https://meetings.aps.org/Meeting/DNP06/Session/DG.6
[4] W. Xiong *et al*, Nature, **575**, 147, 2019
[5] J. Alexander *et al*, report at SLAC meeting, May 2015, https://hallaweb.jlab.org/experiment/APEX/collab15/Cornell_expt_APEX_Collab_Mtg-May2015.pdf, EPJ Web Conf., **142**, 01001, 2017
[6] B. Wojtsekhowski *et al*, JINST 13, 02021 (2018)
[7] M. Raggi and V. Koshuharov, Advances in High Energy Physics, ID959802 (2014), http://dx.doi.org/10.1155/2014/959802
[8] C. Patrignani *et al.* (Particle Data Group), Chin. Phys. **C 40**, 100001 (2016)
[9] B. Wojtsekhowski, "Searching for a U-boson with a positron beam", AIP. Conf. Proc. 1160, 149 (2009), https://doi.org/10.1063/1.3232023
[10] B. Wojtsekhowski, D. Nikolenko and I. Rachek, arXiv:1207.5089, https://arxiv.org/abs/1207.5089
[11] P. Fayet, *Nucl. Phys.* **B347**, 743 (1990)
[12] B. Holdom Phys. Lett. **B178**, (1986), 65
[13] P. Fayet, Phys. Rev. **D 74**, 054034 (2006)
[14] P. Fayet, Phys. Lett. **B 675** (2009) 267-271
[15] P. Fayet, Phys. Rev. **D 75** (2007) 115017
[16] M. Pospelov, Phys. Rev. **D 80**, 095002 (2009)
[17] J.D. Bjorken, R. Essig, P. Schuster, and N. Toro, Phys. Rev. **D80**, 075018 (2009)
[18] N. Arkani-Hamed, D. P. Finkbeiner, T. R. Slatyer, and N. Weiner, Phys. Rev. **D79**, 015014 (2009)
[19] R. Essig, P. Schuster, and N. Toro, Phys. Rev. **D80**, 015003 (2009)
[20] C. Boehm, D. Hooper, J. Silk, M. Casse and J. Paul, Phys. Rev. Lett. **92**, 101301 (2004)
[21] P. Fayet, Phys. Rev. **D 70**, 023514 (2004)
[22] C. Boehm and P. Fayet, *Nucl. Phys.* **B 683** 219 (2004)
[23] N. Borodatchenkova, D. Choudhury, and M. Drees, Phys. Rev. Lett. **96**, 141802 (2006)
[24] Snowmass, Seatle, July 17-26, 2022, https://indico.fnal.gov/event/22303/program
[25] M. Graham, C. Hearty and M. Williams, Annu. Rev. Nucl. Part. Sci. 2021.71:37-58, https://www.annualreviews.org/doi/pdf/10.1146/annurev-nucl-110320-051823
[26] "Dark Sector Physics at High-Intensity Experiments", Report of the RF6 Topical Group for Snowmass 2021, https://arxiv.org/pdf/2209.04671.pdf
[27] M. Williams and S. Gori, Report at Snowmass 2022, https://indico.fnal.gov/event/22303/contributions/245701/attachments/157482/206120/RF6-Report-Discussion.pdf
[28] J. Alexander *et al*, arXiv:1608.08632
[29] M. Battaglieri *et al*, arXiv:1707.04591
[30] J.P. Lees *et al.* (BABAR), Phys. Rev. Lett. **119**, 131804, https://arxiv.org/abs/1702.03327
[31] D. Banerjee *et al.* (NA64), Phys. Rev. Lett. **118**, 011802 (2017)
[32] C. Cazzaniga *et al.* (NA64), Eur. Phys. J. C (2021) 81:959, https://doi.org/10.1140/epjc/s10052-021-09705-5
[33] A.M. Abdullahi *et al*, arXiv:2302.05410, https://arxiv.org/abs/2302.05410
[34] T. Åkesson *et al*, https://arxiv.org/abs/1808.05219; Journal of High Energy Physics, 2020, 4, 3, https://doi.org/10.1007/JHEP04(2020)003
[35] J.P. Lees *et al.* (BABAR), Phys. Rev. Lett. **113**, 201801 (2014)
[36] D. Babusci *et al.* (KLOE-2), Phys. Lett. **B 720**, 111 (2013)
[37] B. Battel, M. Pospelov, and A. Ritz, Phys. Rev. **D80**, 095024 (2009)
[38] R. Essig, R. Harnik, J. Kaplan, and N. Toro, Phys. Rev. **D82**, 113008 (2010)
[39] R. Essig, P. Schuster, N. Toro and B. Wojtsekhowski, **JHEP 02**, 009 (2011)
[40] H. Merkel *et al*, Phys. Rev. Lett. **106**, 251802 (2011)
[41] S. Abrahamyan *et al*, Phys. Rev. Lett. **107**, 191804 (2011)
[42] H. Merkel *et al*, Phys. Rev. Lett. **112**, 221802 (2014)
[43] R. Essig, P. Schuster, N. Toro and B. Wojtsekhowski, E12-10-009, http://hallaweb.jlab.org/experiment/APEX
[44] N. Baltzell *et al*(NPS), NIM-A **859**, 69 (2017), arXiv:1612.07821 [physics.ins-det]; arXiv:2203.08324, https://arxiv.org/abs/2212.10629
[45] A. Gasparian *et al*, JLab experiment E12-21-003, https://www.jlab.org/exp_prog/proposals/22/C12-21-003.pdf
[46] MESA physics program: http://www.prisma.uni-mainz.de/mesa.php
[47] L. Marsicano *et al*, Phys. Rev. Lett. , **121**, 041802 (2018), https://journals.aps.org/prl/abstract/10.1103/PhysRevLett.121.041802
[48] M. Battaglieri *et al*, Eur. Phys. J. A (2021) 57:253, https://doi.org/10.1140/epja/s10050-021-00524-6
[49] M. Freytsis, G. Ovanesyan, and J. Thaler, **JHEP 01**, 111 (2010)
[50] W. Heitler. The Quantum Theory of Radiation, Clarendon Press, Oxford (1954)
[51] Y-S. Tsai, Rev. Mod. Phys **46** 815 (1974), Rev. Mod. Phys **49** 421 (1977

[52] A.B. Arbuzov *et al*, JHEP **10** (1997) 001
[53] F.A. Berends and R. Kleiss, *Nucl. Phys.* **B186** (1981) 22
[54] P. Degtiarenko, DINREG results (private communication).
[55] Primex conceptual design report. `http://www.jlab.org/primex/`, 2000
[56] A. Asaturyan *et al*, "Electromagnetic calorimeters based on scintillating lead tungstate crystals for experiments at Jefferson Lab", NIM-A, **1013**, 165683 (2021)
[57] J. Grames, talk at the Workshop in 3/7, 2023, `https://indico.jlab.org/event/680/`
[58] G. Charpak and F. Sauli, "Multiwire proportional chambers and drift chambers", NIM, **162**, 405, 1979
[59] I. Rachek, in Hall A annual report, `https://hallaweb.jlab.org/publications/AnnualReports/AnnualReport2007.pdf`
[60] F. Ameli *et al*, 2104.11388, `https://arxiv.org/abs/2104.11388`
[61] M. Bondì, Streaming data acquisition system for CLAS12 Forward Tagger, `https://indico.fnal.gov/event/46746/contributions/210438/attachments/141189/177705/CPAD_Bondi.pdf`
[62] Note that the 2γ cross section (1b) can be derived from (2) by setting $\mu = 0$, $\varepsilon = 1$ and multiplying by $1/2$ to account for two identical photons in the final state.